Photocatalytic Synthesis of p-Anisaldehyde in a Mini Slurry-Bubble Reactor under Solar Light Irradiation

Photocatalytic Synthesis of p-Anisaldehyde in a Mini Slurry-Bubble Reactor under Solar Light Irradiation

Dalia Heggo[1,2,3,6], Shinichi Ookawara[2,3*], Teruhisa Ohno[4], Toru Nakai[5], Yoshihisa Matsushita[2], Mona Gamal Eldin[2], Masahiro Ohshima[6]

[1]Department of Chemical Engineering and Pilot plant, National Research Centre, 33 Elbuhouth St., Dokki, 12622, Cairo, Egypt.

[2]Egypt-Japan University of Science and Technology, 179 New Borg El-Arab, Alexandria 21934, Egypt.

[3]Department of Chemical Science and Engineering, Tokyo Institute of Technology, 2-12-1 S1-26, O-okayama, Meguro-ku, Tokyo 152-8552, Japan.

[4]Department of Applied Chemistry, Faculty of Engineering, Kyushu Institute of Technology, 1-1 Sensuicho, Tobata, Kitakyushu 804-8550, Japan.

[5]Corporate Research Center, R & D Headquarters, Daicel Corporation, 1239, Shinzaike, Aboshi-ku, Himeji-shi, Hyogo 671-1283, Japan.

[6]Department of Chemical Engineering, Kyoto University, Nishigyo-ku, Kyoto, 616-8510, Japan.

[*] Corresponding Author: Shinichi Ookawara

Email: sokawara@chemeng.titech.ac.jp

Abstract

Dense photocatalyst slurry was employed for the synthesis of *p*-anisaldehyde under solar light irradiation. An Fe-modified rutile TiO_2 (Fe-TiO_2, 34.5 m^2/g) photocatalyst was used as a visible-light-responsive photocatalyst. A conventional TiO_2 (P25, 35 m^2/g) photocatalyst was also examined as a reference catalyst. XRD pattern and diffuse reflectance spectra showed that Fe-TiO_2 consists of 100% rutile phase and absorbs more visible light compared to P25, respectively. The catalyst powder was suspended in an ethyl acetate solution of *p*-methoxytoluene in the mini-reactor, with oxygen bubbling, under a solar simulator, visible light, and UV LEDs. *p*-Anisaldehyde, as a reaction product, was analyzed by sampling using gas-chromatograph. Regardless of the light source, Fe-TiO_2 always outperformed P25 in terms of both generation rates (GR) of *p*-anisaldehyde and energy requirements (ER). It was demonstrated that the highly dense Fe-TiO_2 slurry was efficient for the synthesis under solar light owing to the small size of the reactor. The small amount of Pt and ZrO_2 cocatalysts significantly enhanced the GR under solar light. By adopting a visible light responsive Fe-TiO_2 photocatalyst, the mini slurry-bubble reactor under solar light achieved a high GR per catalyst mass (CM), which is one to two orders higher than that reported by most previous studies with high-power lamps.

Keywords Photocatalysis; Solar light; Organic synthesis; Titanium dioxide; Mini reactor

INTRODUCTION

p-Anisaldehyde is a well-known chemical compound utilized as an intermediate in the perfumery and pharmaceutical industries [1]. Many chemical processes for *p*-anisaldehyde have been reported in the literature, although those usually involve negative environmental impacts. While significant attention has been paid to its photocatalytic synthesis as an environmentally-friendly alternative, the reaction efficiency was low even with high-power UV light sources [2–5].

Recently, it was reported that the generation rate (GR) of *p*-anisaldehyde per lamp power could be enhanced by employing a mini slurry-bubble reactor with UV LED and a TiO_2 (P25) photocatalyst [6]. However, specialized UV LEDs are costly, and there is a risk of exposure to harmful UV radiation in the process [7]. The previous work by Heggo et al. [8] examined WO_3, a visible-light-responsive photocatalyst for the synthesis of *p*-anisaldehyde under a solar simulator, visible light, and UV LEDs in the similar setup, and found that WO_3 can be applied to this process when using visible light. In this study, an Fe-modified rutile TiO_2 (Fe-TiO_2) visible light responsive photocatalyst was used in the *p*-anisaldehyde synthesis in the mini-reactor under solar and artificial lights. Among many visible light responsive photocatalysts developed in our previous works[9–11], the most potential catalyst was chosen for this work.

To date, the photocatalytic applications of TiO_2 have been extensively studied, because its strong oxidation power and long-term stability make its applications promising [12]. On the other hand, a significant disadvantage of TiO_2 has been its large band gap. Its band gap limits its photosensitivity to UV light which constitutes 3 to 5 % of the sunlight [13].

Doping transitional metals or nonmetals into UV-active metal oxides is an effective way to narrow the band gap. The doping can be attained through impregnation via sol-gel[14], co-precipitation[15] and amalgamation of powders through mechanical mixing[16], chemical vapour

deposition[17], cation exchange[18] and so on [19]. Those dopants can increase photocatalytic efficiency and act as suppressors for the recombination of the photo-induced electron-hole pairs [20]. Among different dopants, Fe^{3+} is frequently employed due to its unique half-filled electron configuration, which narrows the energy gap and may also diminish the recombination of electrons and holes by capturing photo-generated carriers [21]. Recently, Fe^{3+} dopants were used to modify the exposed crystal faces of shape-controlled TiO_2 [9], which worked as visible-light sensitizers while noticeably improving the photocatalytic reaction rate under visible light [22]. The site-selective adsorption on the exposed crystal faces of TiO_2 was attributed to the adsorption characteristics of Fe^{3+} ions [11]. The developed catalyst was examined in this study for the *p*-Anisaldehyde production process.

On the other hand, the role of the cocatalyst in facilitating the rate-limiting half reaction attracted the attention of many researchers. Some of the noble metals used as cocatalysts in photocatalysis are Ag, Pt, Pd, Au, and Ru. Among them, the Pt/TiO_2 composite photocatalyst is the most common system. Compared to the bare TiO_2 photocatalyst, Pt/TiO_2 shows stronger photo-reduction ability where the photo-generated holes can freely diffuse to the surface of TiO_2, and further photo-oxidize organic compounds adsorbed onto its surfaces [23]. Zirconium dioxide (ZrO_2) is also a material used in heterogeneous catalysis [24]. The activity of ZrO_2 in photo-oxidative reactions is generally much lower than that of TiO_2. Although ZrO_2 shows an absorption peak at ~ 250 nm, research showed non-negligible absorption in the near UV range (290–390 nm) [25]. Moreover, photocatalytic reactions could occur under irradiation in this range, without higher energy light [24].

Based on the literature review, the sensitization of UV-reactive TiO_2 in the visible light range by surface modifications and reactivity enhancement by cocatalysts can be a strategy to enhance the photocatalytic process in the given mini slurry-bubble reactor under solar light. It is further

desirable that the adopted catalyst brings about significant reactivity even under artificial light so that the process would be continuously operated at night. Therefore, we examined an Fe-TiO_2 nano-rod with ZrO_2 and Pt cocatalysts as mechanical mixtures for the synthesis of *p*-anisaldehyde in a mini-reactor under solar and artificial lights. The mechanical mixture photocatalyst has already been analyzed by Paredes et al. [26] and Yamaguchi et al. [27]. It was suggested that the cocatalyst in the mixture has a synergistic effect for the adsorption of the pollutant, followed by the transfer of the adsorbed compound to the photocatalyst where the reaction happens. In the mechanical mixture, charges transfer through the contact formed by intermolecular forces, of which the agglomerate size is random and dynamically maintained within a range by continuous agitation preventing gravitational settling at the same time [28]. This is fundamentally related to zeta potential, particle surface Gibbs free energy and stress when its size becomes within the nanoscale level. The thermodynamic stability of phases according to particle size can be classified as follows: ≤ 11 nm, between 11 and 35 nm, ≥ 35 nm for Anatase, Brokite, and Rutile, respectively [29,30]. That may infer the rutile phase tends to agglomerate to reduce its stresses. It is interesting that the mechanical mixture technique maintains the main photocatalyst, its particle size, and crystallinity unchanged, while the total specific surface area of photocatalyst and co-catalysts are higher than those chemically bonded, where the contact area is considered inactive [31].

Although the concept of slurry reactors for photocatalysis was introduced since more than 40 years ago[32], it was a simple way to evaluate the reaction kinetics under the light in a macroscale [33,34]. On the other hand, the recent research is concerned with photocatalytic reactions in microscale reactors [35]. Macroscale reactors usually need much longer reaction time than microscale counterpart; the latter provides better mixing and light utilization, for degradation reactions. However, in the present research, we have two challenges; an intermediate product

selectivity in a consecutive reaction and light harvesting in a highly catalyst-loaded reactor. To attain the higher selectivity, very short space-time in flow microreactor is not appropriate, while the short light path is still preferred for light utilization. Accordingly, this research was implemented by using a dense-slurry mini batch reactor, which can provide a solution to the above issues [36],.

The performance of the catalysts and cocatalysts was evaluated in terms of both the GR of *p*-anisaldehyde and the energy requirements (ER) defined as follows:

$$GR\left[\frac{\mu mol}{h}\right] = \frac{\text{Moles of desired product}}{\text{irradiation time}}$$

$$ER\left[\frac{\text{J}}{\mu\text{mol}}\right] = \frac{\text{Power of light incident onto a reactor surface}\left[\frac{J}{s}\right]}{GR\left[\frac{\mu mol}{h}\right] \times \frac{1}{3600}}$$

By neglecting possible solvent evaporation and mineralization of target material, the apparent conversion, yield, and selectivity typically fell into the range around 41.5, 30.2 and 49.5 %, respectively. In this study, evaluation of catalyst and reactor performance was conducted in terms of the above indices rather than inaccurate apparent conversion and selectivity.

p-anisaldehyde was not purified in this study. Although product separation from the solvent might be achieved by distillation or extraction, it was beyond the scope of this study to develop a feasible separation process.

EXPERIMENTAL METHOD

Chemicals

P25 (35 m^2/g) was obtained from Acros Organics and used as a reference catalyst. The cocatalysts powders ZrO_2 (5 μm) and Pt (2 nm) were obtained Sigma Aldrich and Tanaka Kikinzoku Kogyo, respectively.

p-Methoxytoluene (reactant) and ethyl acetate (solvent) were obtained from Wako Pure Chemical Industries, Ltd., while *p*-anisaldehyde, *p*-anisyl alcohol, and *p*-anisic acid used as standard were obtained from Tokyo Chemical Industry Co., Ltd., Wako Pure Chemical Industries, Ltd., and Kanto Chemical Co., Inc., respectively. All the chemicals were obtained from commercial sources as guaranteed reagents and were used without further purification.

Measurements

The crystal structure of the TiO_2 photocatalyst was examined by X-ray diffraction (XRD) analysis measured with an X-ray diffractometer (X'pert Pro MPD, Philips Co.) with a Cu target Kα-ray (λ = 1.5406 Å). The diffuse reflection spectra of the catalyst were measured using a JASCO V-650 spectrophotometer. A UV light meter (UV-340, Lutron electronic, Taiwan) with a 290–390 nm detection range was used to measure the intensity of the UV light. The spectrum of the visible light LED was measured with an MK350 UPRtek spectrometer. A gas chromatograph (GC-14B, Shimadzu Corporation) was used to analyze the oxidation products of *p*-methoxytoluene. The sample was filtered with a syringe filter to separate the solid particulates before injecting it into the gas chromatograph. Although the filtered catalyst could be regenerated if necessary, by heating it to approximately 420 °C, we opted not to recycle it to avoid contamination [37].

Based on the measurements for each standard sample, the peak positions and areas were attributed to the specific compounds and their respective concentrations. The identified products

were *p*-anisaldehyde, *p*-anisic acid, and negligible amounts of *p*-anisyl alcohol, which was supposed to be an intermediate between *p*-methoxytoluene and *p*-anisaldehyde in the successive oxidation as reported previously [6]. *p*-Anisic acid was considered an oxidation product of *p*-anisaldehyde.

Experimental setup and procedures

The photocatalytic activities were evaluated in terms of the GR of *p*-anisaldehyde from *p*-methoxytoluene in the mini slurry-bubble reactor with oxygen-bubbling using different irradiation sources. As described in a previous study [6], the photocatalytic reaction was carried out in a quartz cell (1×1×4.5 cm) with a long neck, by suspending the photocatalyst powder in 4 mL of *p*-methoxytoluene-ethyl acetate solution (2 wt.%). Fe-TiO_2 (34.5 m^2/g) was prepared as described in the previous work [9], where Fe-TiO_2 used in this study is P-01 samples. Its crystallite size is around 97.2 nm. Rod-shaped Fe-TiO_2 has separate oxidative and reductive faces. Redox reactions proceed preferentially on the specific exposed crystal faces of TiO_2. Therefore, Fe^{3+} are selectively distributed on the oxidative face (111) to enhance its visible light activity [9,10].

A given amount of cocatalyst was added to the mixture and dispersed. Before starting the reaction, the reactant mixture was stirred for 4 h in a sealed bottle in the dark to reach adsorption equilibrium. After the adsorption step, the bottle was replaced by the quartz cell to start the reaction. During the 4 h reaction, oxygen was continuously fed into the mixture through a tube at 5.9 mL/min while the mixture was stirred at 500 rpm to ensure sufficient dispersion of the catalyst powder and oxygen. It was confirmed that the catalyst powder and oxygen gas were well dispersed as the mixture looked uniformly and highly turbid due to a high catalyst loading such as 5 g/L while smaller babbles were observable near wall and liquid surface. It is noted that the superficial

oxygen gas velocity was 0.983 mm/s. The oxygen was fed through a pump from a graduated cylinder where oxygen from the gas cylinder was confined in water as shown in Figure 1.

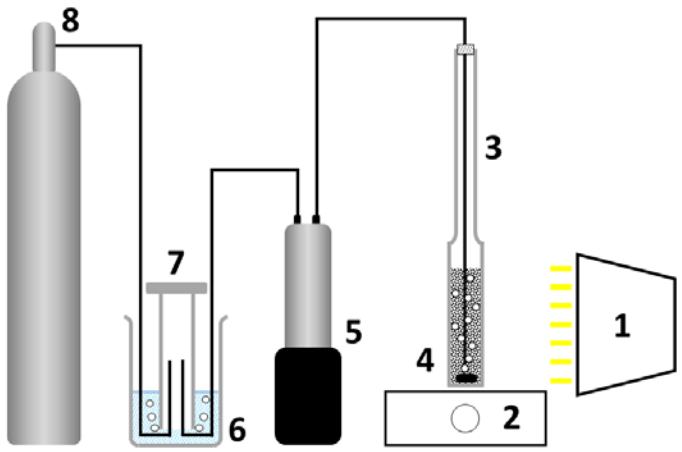

Figure 1 Schematic diagram of experimental setup: 1-irradiation source (UV LED, visible light LED, or solar simulator), 2-magnetic stirrer, 3-quartz cell, 4-stirrer tip, 5-plunger pump, 6- beaker, 7-graduated cylinder, and 8-oxygen gas cylinder.

The three types of light sources are employed as follows: a 12.4 W visible light LED lamp with a circular face (outer diameter, OD = 121 mm) (LDR12N-W, TOSHIBA Co., Japan), a portable solar simulator with an irradiation area of 16 cm^2 (PEC-L01, Peccell) and a UV LED lamp with a peak emission of 361 nm (NLBU21P02, Nichia Corporation, Japan). The distance between the solar simulator and the cell was adjusted to attain a UV intensity of 50 W/m^2 while the distance from the batch cell to the visible light or UV LED was set to 1 cm, which resulted in a UV intensity of 0 and 8.5 kW/m^2, respectively.

Figure 2 shows the spectrum of the visible light LED. It was confirmed that the lamp did not significantly emit UV light (< 400 nm). The manufacturer specified the luminous flux of the lamp and the maximum luminous intensity as 940 lm and 3050 cd, respectively.

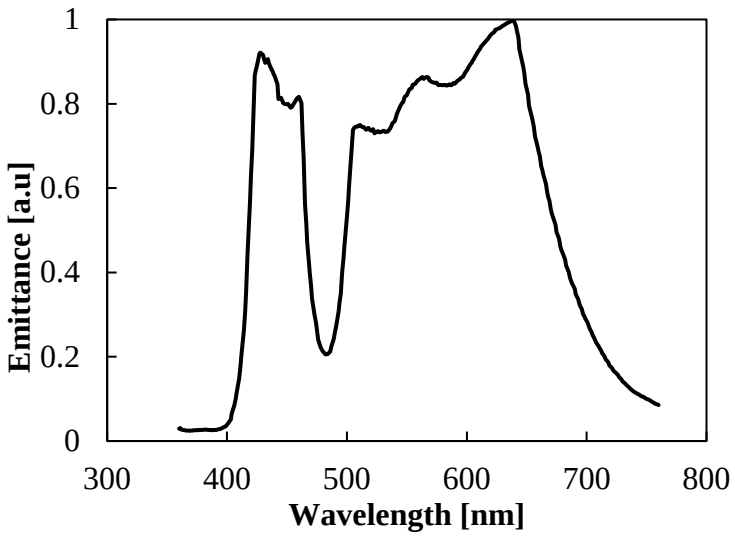

Figure 2 Light emittance spectrum of the visible light LED

RESULTS AND DISCUSSIONS

Characterization of the catalysts and visible light LED

Figure 3 shows the XRD patterns of the examined catalysts. The results indicate that P25 consisted of 87% anatase and 13% rutile, while Fe-TiO_2 consisted of 100% rutile. Iron was not detected because of its small amount as 0.09 wt%. However, Figure 4 shows the deposited Fe on (111) faces of the rutile nanorodes TiO_2. Murakami et al. described the detailed characterization of this catalsyt [38].

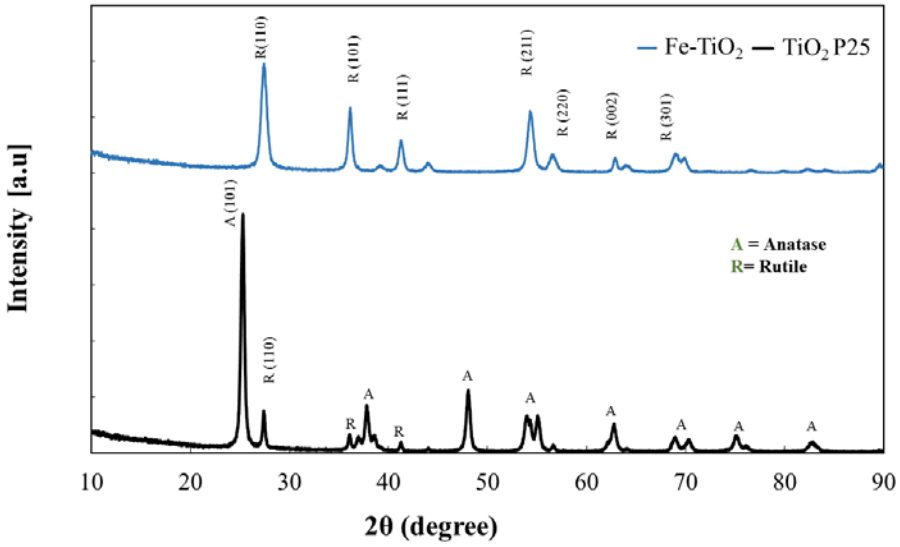

Figure 3 XRD patterns of P25 and Fe-TiO_2

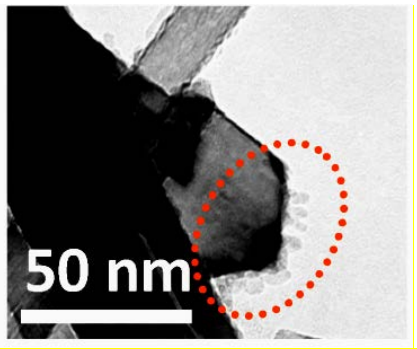

Figure 4 SEM images of Fe modified TiO_2 rutile nanorodes

From the diffusive reflectance spectra of P25 and Fe-TiO_2 shown in Figure 5, we have calculated the band gap values for the samples. The band gaps are determined by extrapolating the steepest lines of each spectrum to x-axis following the previous work [39]. The determined band gaps were 3.05 eV (406 nm) and 2.94 eV (421 nm) for P25 and Fe-TiO_2, respectively. Despite the small band gap difference between both catalysts, Fe-TiO_2 showed a relatively stronger absorption throughout the visible range. The reason is probably that the small amount Fe^{3+} act as a temporary photo-generated electron or hole-trapping site and have a dopant level near the valence band of TiO_2 and reduce the band gap of TiO_2 [28].

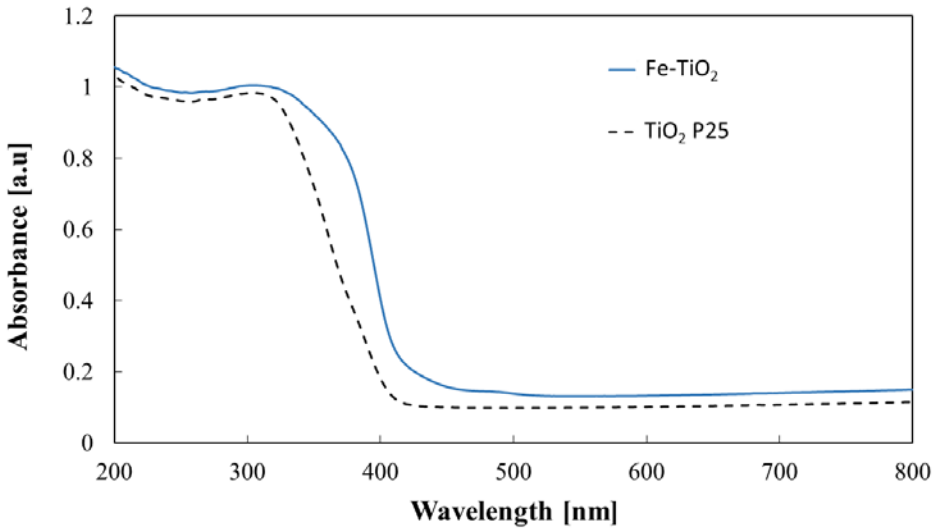

Figure 5 Diffuse reflectance spectra of P25 and Fe-TiO_2

Photocatalytic activity

Effects of light source

The photocatalytic activity was evaluated at first by using the UV LED. It is noted that this reaction did not proceed under the same UV LED without photocatalyst[6]. The loading of each catalyst was adjusted to 5 g/L, based on our previous works [6,8]. As discussed in our previous review and research papers [6, 36], the catalyst loading in photocatalyst slurry reactor was often around 1 g/L in the literature. Such low concentration was typically employed because it is well known that a further increase in the catalyst loading does not result in an increase in reaction rate. However, in a mini batch reactor, because of its shorter light path, the increase in catalyst loading up to 5 g/L or even higher still brought about the increase in reaction rate as shown in our previous work [8]. Therefore, we adopted this catalyst loading in this study. The concentration of *p*-anisaldehyde initially increased with irradiation time, and reached a maximum after 1 and 3 h for

Fe-TiO_2 and P25, respectively. The GR of *p*-anisaldehyde was obtained by dividing the maximum generated number of mol of *p*-anisaldehyde by their corresponding irradiation time. With other light sources, GR was obtained after 4 h of irradiation because the concentration of *p*-anisaldehyde always reached the maximum after 4 h of irradiation.

The ER to generate the same amount of *p*-anisaldehyde was obtained by dividing the electrical power consumed by the lamp by the number of mol of *p*-anisaldehyde at a given irradiation time when the maximum concentration was reached. It should be noted that the surface area ratio of the reactor to a visible light LED lamp face was taken into account to evaluate the power of light incident onto the reactor surface.

Figure 6 shows that Fe-TiO_2 outperformed P25 in terms of both GR and ER regardless of the light source examined. The maximum relative standard deviation (RSD) for each catalyst is provided in the captions of Figures 6–9. The GR of Fe-TiO_2 was significantly higher under UV light with extremely high-intensity. The results can be attributed to the energy level of atomic arrangement of Fe-TiO_2, and crystal faces where oxidation and reduction co-occur , and suppresses recombination probabilities [40].

On the other hand, only Fe-TiO_2 showed a noticeable GR under visible light LED illumination while the reactivity of P25 was negligible. As mentioned above, because of iron ions reactivity over the visible region, can extend the charge-carrier lifetime to minutes and even hours, which is 30 ns for effective TiO_2 [19,41,42].

However, in terms of ER, the visible light LED outperformed the UV LED for Fe-TiO_2. This would be valuable information when selecting the artificial light source for this process. Under moderate solar light, Fe-TiO_2 showed a slightly higher GR compared to P25. Taking into account

the high reactivity of Fe-TiO_2 under intense visible and UV light, the operation of the concentrated solar light could be of further interest.

The next section examines the enhancement of GR by the cocatalysts under solar light.

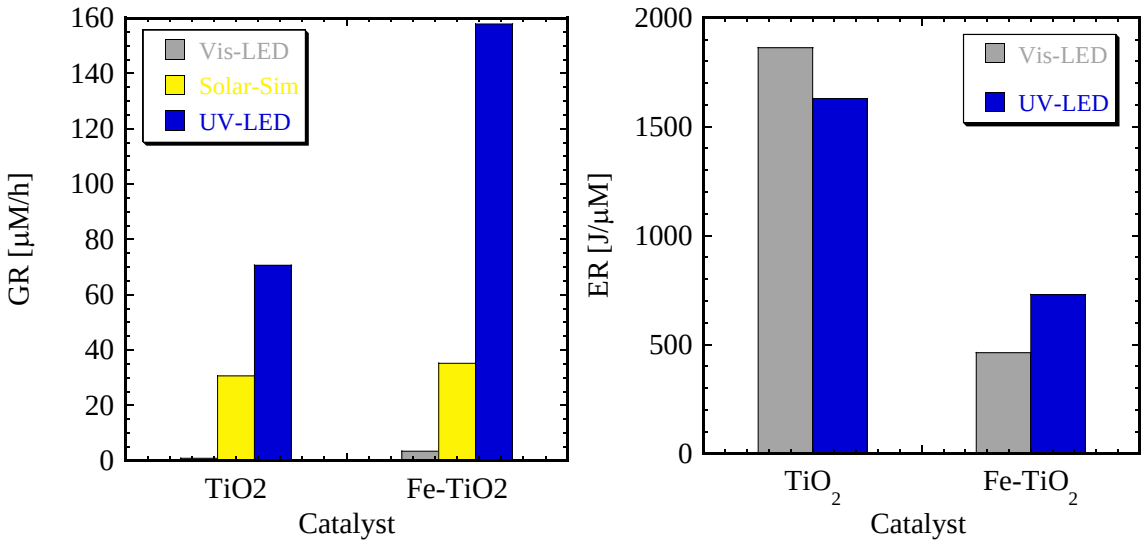

Figure 6 GR and ER for the production of *p*-anisaldehyde under different light sources

(TiO_2, Max. RSD = 0.01, n = 3; Fe-TiO_2, Max. RSD = 0.05, n = 3)

Enhancement of Fe-TiO_2 efficiency under solar light

Effect of catalyst loading

Figure. 7 shows that GR of Fe-TiO_2 under solar light increased as the catalyst loading increased from 1.25 to 10 g/L. This result was remarkable because the photocatalyst concentration in the slurry-bubble reactors was typically adjusted in the range of 0.3 to 3 g/L for the 100 to 1000 mL reactor vessels as found in the literature [36]. In the larger photocatalytic reactors, high catalyst loading is usually avoided, because it results in high turbidity leading to lower reaction rates. On the other hand, in the mini-reactor employed in this study, its small dimensions enabled sufficient

light harvesting and activation of the suspended catalysts over the entire reactor volume despite the high turbidity. Therefore, GR increased as the catalyst loading increased up to 10 g/L.

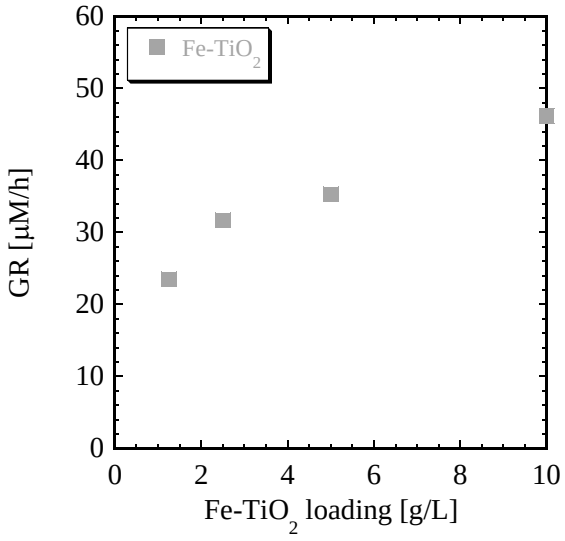

Figure 7 Effect of Fe-TiO_2 catalyst loading on the generation rate of *p*-anisaldehyde (Max. RSD = 0.05, n = 3)

Effect of ZrO_2 loading

The effect of ZrO_2 on GR was examined with a fixed Fe-TiO_2 loading (5 g/L). As seen in Figure 8, the highest GR was obtained for a ZrO_2 loading of 0.5 g/L, where the increase in GR was 27.5 %. It should be noted that the catalytic activity of ZrO_2 (5 g/L) under the visible light LED was as low as 0.124 μmol/h in terms of GR. Therefore, ZrO_2 probably works as an adsorption and stock center for *p*-methoxytoluene, which can enhance the reactant transport to Fe-TiO_2 in the agglomeration of ZrO_2 and Fe-TiO_2. Another possibility is that ZrO_2 might work as an adsorption center for *p*-anisaldehyde, which can enhance the product desorption from Fe-TiO_2 preventing its further oxidation and the adsorption of a new reactant. If ZrO_2 does not function as a catalyst, it will

merely prevent the light from reaching the catalysts by absorbing and scattering it. Such adverse effects seem to be more dominant at higher ZrO_2 loading.

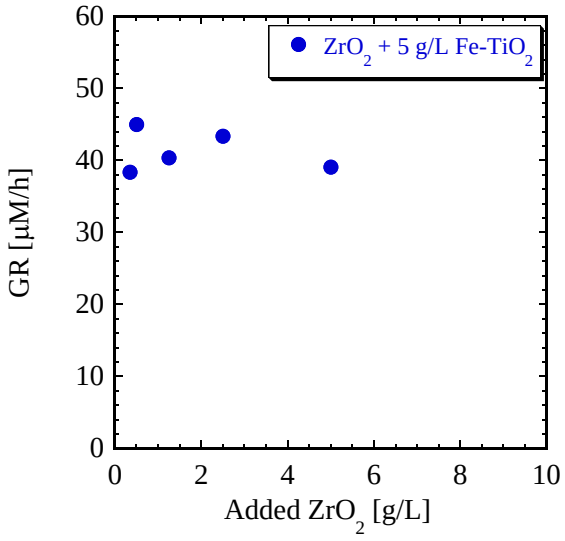

Figure 8 Effect of ZrO_2 cocatalyst loading on the generation rate of *p*-anisaldehyde (Max. RSD = 0.05, n = 3)

Effect of Pt loading

The effect of Pt on GR was examined by loading a given amount of Pt on the best mixture of ZrO_2 (0.5 g/L) and Fe-TiO_2 (5 g/L). It is noted that Pt and ZrO_2 alone were found to be unreactive under the same conditions. As seen in Figure 9, an amount of Pt, smaller than 0.2 g/L brought about an increase of GR up to 31.3%. In the data shown in Figure 9, an average of three reproducible results was obtained for each point with a maximum RSD of 0.02. Platinum particles can act as electron-hole separation centers, while fine Pt particles can provide an unsaturated catalytic surface, where active photocatalytic reactions occur as initiated by either the electrons, holes or both diffusing over the surface [43]. However, the high loading of Pt leads to the formation of Pt clusters, which

may act as electron-hole recombination centers [23]. Such characteristics of Pt seemed to result in the severe decline of GR at higher Pt loading.

Of all the conditions examined, the best results were achieved when adding 0.5 g/L ZrO_2 and 0.2 g/L Pt cocatalysts to 5 g/L Fe-TiO_2. This combination brought ~ 67.4% increase in GR.

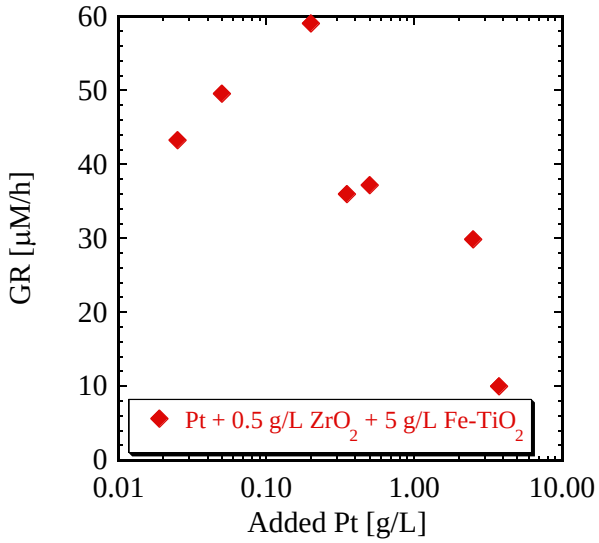

Figure 9 Effect of Pt cocatalyst loading on GR of *p*-anisaldehyde

(Max. RSD = 0.02, n = 3)

Performance comparison with previous studies

The performance of the present reaction system was compared to those of similar systems previously described in the literature in terms of GR per catalyst mass (CM) (GR/CM) and ER. The results are shown in Table 1. In the present study, the highest GR/CM of 7.9 mol/kg·h was achieved with 5 g/L Fe-TiO_2 under a UV LED at an ER of 730 J/μmol. Farhadi et al. [44] achieved the second best GR/CM of 3.7 mol/kg·h using a 400 W mercury lamp resulting in an ER of 1600 J/μmol. The present study achieved the third best GR/CM of 2.6 mol/kg·h even under solar light. It is remarkable that such a high GR/CM can be achieved under solar light since the value was one to two orders higher than the values attained in the previous studies using high power lamps.

In terms of ER, our previous work achieved the best performance with 5 g/L WO_3 using the same visible light LED. Overall, the comparison proved that the mini slurry-bubble reactor could achieve high generation rates of *p*-anisaldehyde even under solar light by highly loading a Fe-TiO_2 with optimized amounts of ZrO_2 and Pt cocatalysts. This reaction system can also operate under artificial lights with minimum ER, i.e., minimum production costs at night, compared to the previous reaction systems described in the literature.

Table 1 Comparison of reaction system performance with respect to GR and ER

	Irradiation time [h]	GR/CM [mol/kg·h]	ER [J/µmol]
Present study			
5.7 g/L (Pt+ZrO_2+ Fe-TiO_2) under solar light	4	2.6	0
5 g/L Fe-TiO_2 under Vis LED	4	0.17	460
5 g/L Fe-TiO_2 under UV LED	1	7.9	730
Our previous study [45]			
5 g/L WO_3 under solar light	4	0.13	0
5 g/L WO_3 under Vis LED	4	0.35	230
5 g/L WO_3 under UV LED	3	0.84	6 800
References			
Bouquet-somrani et al. [46]	48	0.03	18 000
El-bery et al. [47]	4	0.14	8 300
Palmisano et al. [48]	7.7	0.02	23 000
Addamo et al. [49]	4.3	0.05	55 000
Farhadi et al. [44]	1	3.7	1 600
Augugliaro et al. [50]	8.8	0.9	2 600
Yurdakal et al. [12]	2.36	0.3	7 500
Yurdakal et al. [51]	2.6	0.23	6 600
Yurdakal et al. [52] Visible light	1.8	0.05	86 000

	near UV light	0.35	0.7	8 800
Qamar et al. [53]		2.5	0.6	23 000

4 Conclusions

In this study, the photocatalytic synthesis of *p*-anisaldehyde in the mini slurry-bubble reactor was successfully intensified by highly loading a Fe-TiO_2 nanorod with ZrO_2 and Pt cocatalysts, under solar light.

It was remarkable that Fe-TiO_2 with ZrO_2 and Pt cocatalysts showed a high *p*-anisaldehyde GR even under solar light. The GR was one to two orders higher compared to those reported in similar previous studies using high power lamps, such as a 400 W mercury lamp. The optimized composition, which attained a 67.4% increase in GR compared to Fe-TiO_2 alone under solar light, was 5 g/L Fe-TiO_2, 0.5 g/L ZrO_2, and 0.2 g/L Pt, respectively. The high performance of the mini slurry-bubble reactor is mainly attributed to its small dimension that enabled sufficient light harvesting over the reactor volume. Therefore, the further intensification of this photocatalytic process will be expected by downsizing the reactor if technical difficulties can be overcome.

The operation of the present reaction system under concentrated solar light should undergo further improvement of reactor performance because the adopted Fe-TiO_2 photocatalyst showed the highest reactivity under intense UV and visible light rather than under moderate solar light compared with P25.

In the future, the existing limitations such as solvent evaporation, uneven light distribution over the reactor, and not-optimized reaction time in conjunction with selectivity should be addressed.

Acknowledgments: The authors would like to thank the analysis center from the Tokyo Institute of Technology, the Egyptian Ministry of Higher Education and Egypt-Japan University of Science and Technology (E-JUST) for their support to this study.

Declarations of interest: None

FIGURE AND TABLE CAPTIONS

Figure 1 Schematic diagram of the experimental setup: 1-irradiation source (UV LED, visible light LED, or solar simulator), 2-magnetic stirrer, 3-quartz cell, 4-stirrer tip, 5-plunger pump, 6-beaker, 7-graduated cylinder, and 8-oxygen gas cylinder.

Figure 2 Light emittance spectrum of the visible light LED

Figure 3 XRD patterns of P25 and Fe-TiO_2

Figure 4 SEM images of Fe modified TiO_2 rutile nanorodes

Figure 5 Diffuse reflectance spectra of P25 and Fe-TiO_2

Figure 6 GR and ER for the production of *p*-anisaldehyde under different light sources

(TiO_2, Max. RSD = 0.01, n = 3; Fe-TiO_2, Max. RSD = 0.05, n = 3)

Figure 7 Effect of the Fe-TiO_2 catalyst loading on the generation rate of *p*-anisaldehyde

(Max. RSD = 0.05, n = 3)

Figure 8 Effect of the ZrO_2 cocatalyst loading on the generation rate of *p*-anisaldehyde

(Max. RSD = 0.05, n = 3)

Figure 9 Effect of the Pt cocatalyst loading on the GR of *p*-anisaldehyde

(Max. RSD = 0.02, n = 3)

Table 1 Comparison of reaction system performance with respect to GR and ER

References

[1] F. M. Bautista, D. Luna, J. Luque, J. M. Marinas, J. F. Sánchez-Royo, *Appl. Catal. A Gen.* **2009**, *352*, 251.

[2] J. Jiang, B. Wu, C. Cha, *Electrochim. Acta* **1998**, *43*, 2549.

[3] H. M. Alvarez, D. P. Barbosa, A. T. Fricks, D. A. G. Aranda, R. H. Valdes, O. A. C. Antunes, *Org. Process Res. Dev.* **2006**, *10*, 941.

[4] U. Bentrup, A. Martin, G.-U. Wolf, *Catal. Today* **2003**, *78*, 229.

[5] B. M. Reddy, K. N. Rao, G. K. Reddy, P. Bharali, *J. Mol. Catal. A Chem.* **2006**, *253*, 44.

[6] D. Heggo, H. Mohamed, S. Ookawara, Y. Matsushita, *J. Chem. Eng. Japan* **2016**, *49*, 130.

[7] M. R. Krames, O. B. Shchekin, R. Mueller-mach, G. O. Mueller, L. Zhou, G. Harbers, M. G. Craford, *J. Disp. Technol.* **2007**, *3*, 160.

[8] D. Heggo, S. Ookawara, D. Fukushi, A. Sato, Y. Matsushita, M. Ohshima, M. G. ElDin, "Photocatalytic Synthesis of p-Anisaldehyde by Using WO3 under visible light," Asia Pacific Confederation of Chemical Engineering Congress 2015: APCChE 2015, incorporating CHEMECA 2015, Engineers Australia, Melbourne, **2015**.

[9] N. Murakami, A. Ono, M. Nakamura, T. Tsubota, T. Ohno, *Appl. Catal. B Environ.* **2010**, *97*, 115.

[10] E. Bae, N. Murakami, T. Ohno, *J. Mol. Catal. A Chem.* **2009**, *300*, 72.

[11] T. Ohno, D. Haga, K. Fujihara, K. Kaizaki, M. Matsumura, *J. Phys. Chem. B* **1997**, *101*, 6415.

[12] S. Yurdakal, G. Palmisano, V. Loddo, V. Augugliaro, L. Palmisano, *Am. Chem. Soc.* **2008**, *130*, 1568.

[13] U. Diebold, *Surf. Sci. Rep.* **2003**, *48*, 53.

[14] M. Behnajady, N. Modirshahla, M. Shokri, B. Rab, *Glob. Nest J.* **2008**, *10*, 1.

[15] T. Sreethawong, Y. Suzuki, S. Yoshikawa, 4.

[16] K. Hashimoto, K. Wasada, M. Osaki, E. Shono, K. Adachi, N. Toukai, H. Kominami, Y. Kera, *Appl. Catal. B Environ.* **2001**, *30*, 429.

[17] Z. Ding, X. Hu, P. L. Yue, G. Q. Lu, P. F. Greenfield, *Catal. Today* **2001**, *68*, 173.

[18] S. Anandan, M. Yoon, *J. Photochem. Photobiol. C Photochem. Rev.* **2003**, *4*, 5.

[19] O. Carp, C. L. Huisman, A. Reller, *Prog. Solid State Chem.* **2004**, *32*, 33.

[20] X. Cheng, X. Yu, Z. Xing, J. Wan, *Energy Procedia* **2012**, *16*, 598.

[21] Y. Liu, J. H. Wei, R. Xiong, C. X. Pan, J. Shi, *Appl. Surf. Sci.* **2011**, *257*, 8121.

[22] N. Murakami, T. Chiyoya, T. Tsubota, T. Ohno, *Appl. Catal. A Gen.* **2008**, *348*, 148.

[23] F. Li, X. Li, *Chemosphere* **2002**, *48*, 1103.

[24] J. A. Navio, G. Colón, J. M. Herrmann, *J. Photochem. Photobiol. A Chem.* **1997**, *108*, 179.

[25] J. A. Navío, G. Colón, M. Macías, P. J. Sánchez-Soto, V. Augugliaro, L. Palmisano, *J. Mol. Catal. A Chem.* **1996**, *109*, 239.

[26] S. P. Paredes, M. A. Valenzuela, G. Fetter, S. O. Flores, *J. Phys. Chem. Solids* **2011**, *72*, 914.

[27] K. Yamaguchi, K. Inumaru, Y. Oumi, T. Sano, S. Yamanaka, *Microporous Mesoporous*

Mater. **2009**, *117*, 350.

[28] S. U. Ilyas, R. Pendyala, N. Marneni, *Mater. Res. Innov.* **2014**, *18*, S6.

[29] S. G. Kumar, K. S. R. K. Rao, *Nanoscale* **2014**, *6*, 11574.

[30] D. A. H. Hanaor, C. C. Sorrell, *J. Mater. Sci.* **2011**, *46*, 855.

[31] Y. Kim, H. Irie, K. Hashimoto, *Appl. Phys. Lett.* **2008**, *92*, 182107.

[32] D. S. Hacker, J. B. Butt, *Chem. Eng. Sci.* **1975**, *30*, 1149.

[33] C.-H. Wu, H.-W. Chang, J.-M. Chern, *J. Hazard. Mater.* **2006**, *137*, 336.

[34] J. Moreira, B. Serrano, A. Ortiz, H. de Lasa, *Ind. Eng. Chem. Res.* **2010**, *49*, 10524.

[35] R. Gorges, S. Meyer, G. Kreisel, *J. Photochem. Photobiol. A Chem.* **2004**, *167*, 95.

[36] D. Heggo, S. Ookawara, *Chem. Eng. Sci.* **2017**, *169*, 67.

[37] L. Cao, Z. Gao, S. L. Suib, T. N. Obee, S. O. Hay, J. D. Freihaut, *J. Catal.* **2000**, *196*, 253.

[38] N. Murakami, A. Ono, M. Nakamura, T. Tsubota, T. Ohno, *Appl. Catal. B Environ.* **2010**, *97*, 115.

[39] H. Li, Synthesis of Titanium Dioxide Photocatalyst with Tunable Nanoporosity Using Supercritical Fluids, University of South Florida, **2013**.

[40] E. Bae, N. Murakami, T. Ohno, *J. Mol. Catal. A Chem.* **2009**, *300*, 72.

[41] A. R. Bally, E. N. Korobeinikova, P. E. Schmid, F. Lévy, F. Bussy, *J. Phys. D. Appl. Phys.* **1998**, *31*, 1149.

[42] F. C. Gennari, D. M. Pasquevich, *J. Mater. Sci.* **1998**, *33*, 1571.

[43] D. Riassetto, C. Holtzinger, M. Langlet, *J. Mater. Sci.* **2009**, *44*, 2637.

[44] S. Farhadi, M. Afshari, M. Maleki, Z. Babazadeh, *Tetrahedron Lett.* **2005**, *46*, 8483.

[45] "Photocatalytic Synthesis of p-Anisaldehyde by Using WO3 under visible light," AU, **2015**.

[46] C. Bouquet-somrani, A. Finiels, P. Geneste, P. Graffin, *Catal. Letters* **1995**, *33*, 395.

[47] H. El-bery, Y. Matsushita, A. Abdel-moneim, “One Step Photocatalytic Selective Oxidation of p - Methoxy Toluene over TiO2 / Graphene Composite in Comparison of Pure TiO2,” World Congress on New Technologies (NewTech 2015), Barcelona, **2015**.

[48] G. Palmisano, S. Yurdakal, V. Augugliaro, V. Loddo, L. Palmisano, *Adv. Synth. Catal.* **2007**, *349*, 964.

[49] M. Addamo, V. Augugliaro, M. Bellardita, A. Di Paola, V. Loddo, G. Palmisano, L. Palmisano, S. Yurdakal, *Catal. Letters* **2008**, *126*, 58.

[50] V. Augugliaro, V. Loddo, M. J. López-Muñoz, C. Márquez-Alvarez, G. Palmisano, L. Palmisano, S. Yurdakal, *Photochem. Photobiol. Sci.* **2009**, *8*, 663.

[51] S. Yurdakal, G. Palmisano, V. Loddo, O. Alagöz, V. Augugliaro, L. Palmisano, *Green Chem.* **2009**, *11*, 510.

[52] S. Yurdakal, V. Augugliaro, V. Loddo, G. Palmisano, L. Palmisano, *New J. Chem.* **2012**, *36*, 1762.

[53] M. Qamar, R. B. Elsayed, K. R. Alhooshani, M. I. Ahmed, D. W. Bahnemann, *ACS Appl. Mater. Interfaces* **2015**, *7*, 1257.